Oxygen reduction reaction activity and surface properties of nanostructured nitrogen-containing carbon

Paul H. Matter, Eugenia Wang, Maria Arias, Elizabeth J. Biddinger, Umit S. Ozkan*

Department of Chemical Engineering, The Ohio State University, Columbus, OH 43210, United States

Abstract

Nitrogen-containing carbon nanostructures were prepared from the decomposition of acetonitrile at 900 °C over silica and magnesia supports impregnated with Fe, Co, or Ni. For the carbon grown from supported Fe and Co particles, compartmentalized fibers with a stacked cup structure predominantly formed, while mostly broken multi-walled nanotubes formed from Ni particles. The fibers were purified from the support by removing silica with 1 M KOH, or removing metal particles and magnesia with 1 M HCl. Surface analysis was performed with XPS and hydrophobicity comparisons. Surface properties were related to nanostructure and edge plane exposure. Activity for the ORR was highest over CN_x fibers grown from supported Fe and Co particles, which may also be related to edge plane exposure, and not necessarily to the presence of metal contamination. The most active materials were generally the most selective catalysts as well. Moreover, from Tafel plot slopes a trend was observed depending on the precursor metal used to prepare the CN_x. The magnitude of the Tafel slope was smallest for the samples prepared from Fe or Co precursors. Compared to a state-of-the-art platinum catalyst, the most active alternative non-noble metal catalysts had less than 100 mV potential drop difference, high selectivity for complete oxygen reduction, a similar Tafel slope, and good electrical conductivity.
© 2006 Elsevier B.V. All rights reserved.

Keywords: Oxygen reduction reaction (ORR); Nitrogen containing carbon; Nanostructured carbon; PEM fuel cell cathode

1. Introduction

The development of alternative catalysts to platinum is a high priority for proton exchange membrane (PEM) fuel cells. Currently, the high loading requirements for platinum in the cathode of PEM fuel cells will limit the ability to commercialize this technology in the automotive industry [1,2]. Promising catalysts prepared from pyrolyzed iron, nitrogen, and carbon precursors have shown good performance compared to platinum [3,4]. A thorough review of alternative catalyst work to date is given elsewhere [5]. To summarize briefly, in the 1960s alternative catalysts with an organic macrocycle active site were developed [6,7]. In this class of catalysts, a transition metal (usually Fe or Co) is stabilized by nitrogen species that are part of the macrocycles, similar to the active site in hemoglobin. However, these materials have poor stability in the fuel cell environment [8,9]. Since that time, it was discovered that active and more stable ORR catalysts can be prepared from the pyrolysis of these

organic macrocycles, or from the pyrolysis of various other precursors that contain iron, nitrogen, and carbon [10–20]. There has been debate over whether the role of the transition metal is as a catalyst for the formation of active sites during the heat treatments, or as part of the active site itself [5].

Recently, nitrogen-doped carbon (CN_x) fibers grown from pure alumina or supported Fe have proven to be highly active catalysts for the oxygen reduction reaction (ORR) in a PEM fuel cell environment [21–23]. Compared to other alternative cathode catalysts, the nanostructured CN_x fibers perform well, and have good potential for replacing platinum as ORR catalysts [5]. Reports have shown that active ORR catalysts can be prepared from the pyrolysis of nitrogen and carbon precursors in the presence of iron particles supported by carbon [23] or alumina [21,22], in the form of unsupported volatile organometallic compounds [24], or even in the original form of an organic macrocycle [25]. The key requirement for high activity was found to be that the fibers formed have a high degree of edge exposure. Since active catalysts could be prepared without any transition metal, it was determined that nitrogen-doped carbon is itself active for the ORR, and the transition metal typically added for improved activity is a catalyst for the formation

* Corresponding author. Tel.: +1 614 292 6623; fax: +1 614 292 3769.
E-mail address: ozkan.1@osu.edu (U.S. Ozkan).

of more edge planes during the pyrolysis. Thus the transition metal may or may not be part of an active site itself.

In the previous paper of this series, we reported the preparation of CN_x fibers from the pyrolysis of acetonitrile at 900 °C over Fe, Co, and Ni particles supported by SiO_2 or MgO [26]. This work demonstrated a simple method to prepare CN_x nanofibers. A variety of fiber diameters, fiber types, and nitrogen contents could be prepared using different metal/support combinations. Fibers prepared from Fe and Co particles generally had structures that should yield a high percentage of edge planes exposed, thus it is expected that these materials could perform well as ORR catalysts. In this study we further examine the nanostructure, and the surface properties of these materials, such as nitrogen species present and hydrophobicity. Moreover, electrochemical properties will be examined, such as conductivity, activity for the ORR, and selectivity for complete oxygen reduction to water. Relations between nanostructure, surface properties, and electrocatalytic activity are discussed.

2. Experimental

2.1. Catalyst preparation

The sample preparation and carbon purification was described in detail in the previous paper of this series [26]. Briefly, all of the CN_x fibers were grown from supported metal particles at 900 °C using acetonitrile vapors. Both silica and magnesia were used as supports for Fe, Co, and Ni particles. To remove silica, the fibers were washed with KOH, and to remove the metal particles and/or MgO, the fibers were washed with HCl.

2.2. TEM

Transmission electron microscopy was performed with a Philips Tecnai TF20. Samples were supported by lacey-formvar carbon on a 200 mesh copper grid. The samples were dispersed with excess ethanol before being deposited on the support.

2.3. XPS

X-ray photoelectron spectroscopy analysis was performed using a Kratos Ultra Axis Spectrometer on samples to determine surface composition of the elements present, and to gain insight about the nature of functional groups on the surface. Each sample was palletized and placed on a stainless steel disk for analysis. For each sample a survey was performed from 1200 to 0 eV using an Al anode at 13 kV, and a 10 mA current. Next, five sweeps were carried out for each element concurrently, with the C 1s, N 1s, and O 1s region always being scanned in addition to the respective metal and support regions.

2.4. Conductivity and activity testing

The procedure for conductivity and activity testing is reported elsewhere [21]. Briefly, the activity of all samples for the ORR was gauged with cyclic voltammetry (CV) experiments using a PAR Bi-Stat with a model 636 rotating ring-disk electrode (RRDE) set-up. A catalyst ink was prepared using one part (by mass) of catalyst and 11 parts of 0.5 wt% Nafion in aliphatic alcohols. After sonicating the ink, approximately 10 μL was dispensed on the glassy carbon disk so as to completely cover the glassy carbon current collector with a thin film of catalyst, but not cover the platinum ring or Teflon casing of the RRDE. The inks were also used for conductivity measurements, described elsewhere [23]. In the conductivity testing set-up, samples were subjected to 100 psi of pressure. Vulcan carbon XC-72 (as received) had a conductivity of 71 S/m in this set-up.

For the activity testing, a 0.5 M solution of H_2SO_4 was used as the electrolyte. Gas was removed from the catalyst pores during an initial test sweep from 1.2 to 0 V (versus NHE) at 10 mV/s in the O_2 sparged electrolyte, thus allowing the pores to fill with solution. This step was found to be necessary to ensure good background reproducibility after the sparging steps. Next, the solution was sparged with argon, and five consecutive CVs were run on the disk from 1.2 to 0.0–1.2 V (versus NHE) at 50 mV/s. Then, a baseline for the disk was obtained by sweeping from 1.2 to 0.0–1.2 V (versus NHE) at 10 mV/s in the argon sparged solution at a 100 rpm rotation rate. Simultaneously, a background for the ring was obtained while holding the voltage of the Pt ring at 1.2 V versus NHE. Finally, the solution was saturated with O_2 and slow CVs (10 mV/s) were then taken at rotations of 0, 100, and 1000 rpm. The peak in reduction current on the disk during the sweep without rotation is reported as a measurement of ORR activity. During the CV at 100 rpm, the ring potential was held at 1.2 V versus NHE, and its current was monitored to detect any H_2O_2 production originating from the sample (on the disk). A higher amount of current in the ring indicates higher selectivity of the sample to peroxide, an undesirable byproduct. The RRDE manufacturer reports the collection efficiency of the ring to be 20% under laminar flow conditions. The reported ring currents were multiplied by 5 to correct for this efficiency.

2.5. TPO

Temperature programmed oxidation of samples was carried out using a Setaram TG-DSC 111 with the product stream being analyzed by a Cirrus mass spectrometer (MS). Approximately 10 mg of sample was loaded into the TGA and the temperature was ramped at 5 °C/min to 750 °C in 10% O_2 in He flowing at 60 sccm (split evenly between the reference and sample side). Both the TG and DSC signals were recorded. The MS was used to follow oxides of nitrogen and carbon that formed from the combustion. Products were quantified using ionization probabilities provided by the instrument manufacturer.

3. Results

Previously, we have reported the preparation and bulk characterization of nitrogen-doped carbon nanofibers from metal particles (Fe, Co, or Ni) supported by silica or magnesia using acetonitrile as the feedstock. During this study, it was observed that amorphous carbon and short graphitic ribbons
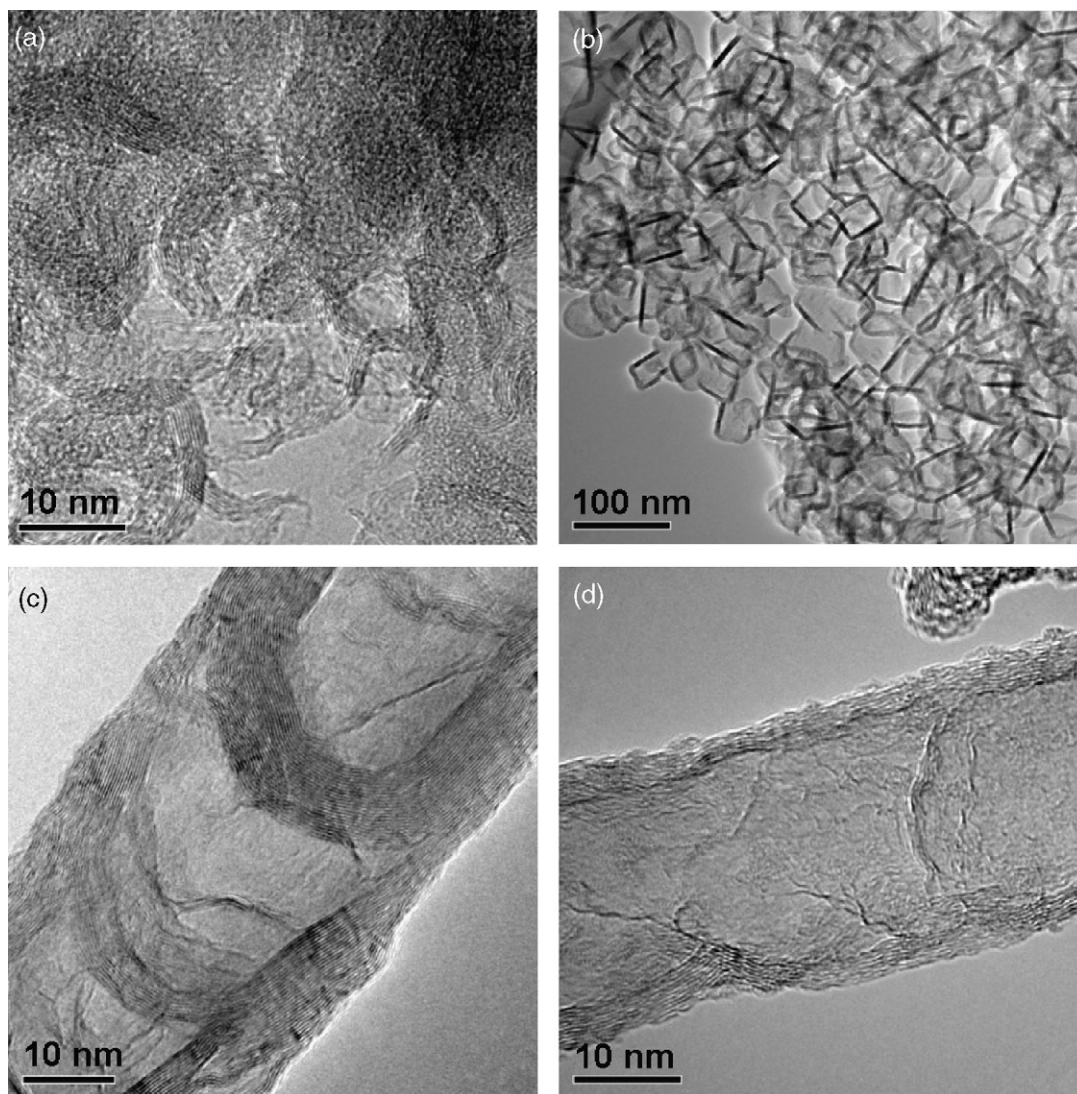
Fig. 1. TEM images representative of CN_x structures formed from (a) pure SiO_2, (b) pure MgO, (c) Fe or Co particles, and (d) Ni particles.

formed in the silica sample while shells of nitrogen-containing carbon (CN_x) formed on the cubic magnesia crystals. Following acetonitrile pyrolysis, the supports were washed away with KOH or HCl, respectively, to leave behind the CN_x in a purified form. TEM images of the CN_x formed over SiO_2 and MgO supports are shown in Fig. 1a and b, respectively. On the other hand, supported Fe and Co particles catalyzed the formation of compartmentalized fibers with a stacked cup structure. An example of this structure is shown in Fig. 1c. The supported Ni particles catalyzed the formation of mostly multi-walled nano-tubes (MWNTs) and broken MWNTs (see Fig. 1d as an example). These different fiber types were also obtained from alumina-supported Fe or Ni, respectively. The fibers formed from alumina-supported Fe had high activity for the oxygen reduction reaction in addition to unique surface properties compared to the Ni-derived CN_x fibers, therefore, we will examine ORR activity of the magnesia- and silica-derived CN_x and any potential relation to surface properties.

3.1. XPS surface characterization

To characterize the composition of the sample surfaces, all of the nitrogen-doped carbon materials prepared were analyzed by XPS. The C 1s, N 1s, and O 1s regions were scanned in addition to the appropriate regions for the support, the metal, and the washing agent. An example of C 1s, N 1s, and O 1s regions are shown in Fig. 2. The C 1s peak is shifted to a binding energy higher than expected for pure carbon and has a prominent higher binding energy shoulder. These effects are common for nitrogen-doped carbon [11]. The N 1s region was deconvoluted into three peaks. The two most stable species present in carbon heated to 900 °C are pyridinic (398.6 ± 0.3 eV) and quarternary (401.2 ± 0.2 eV) nitrogen. All of the samples had some contribution from these species. It should be mentioned that pyridinic nitrogen is a type of nitrogen that can only be found on the edge of a carbon plane. The quarternary nitrogen peak had a higher binding energy shoulder that was fit to a third peak. It is possible that this shoulder is similar in nature to the C 1s higher binding
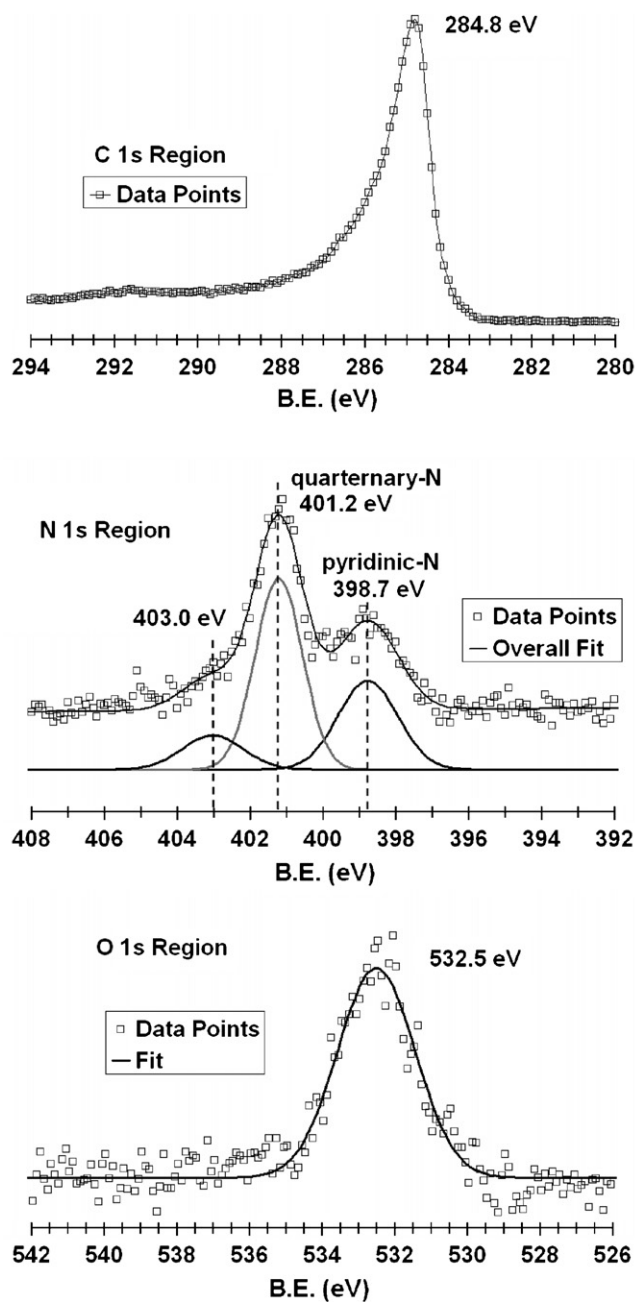
Fig. 2. XPS spectra of C 1s, N 1s, and O 1s regions for CN_x prepared from 2% Fe/SiO_2.

Table 1
XPS analysis results for CN_x formed from acetonitrile pyrolysis over silica supports

Region	BE (eV)	Composition (%)
SiO$_2$–KOH washed		
O 1s	532.9	27.2
N 1s	401.1	3.5
N 1s	398.6	1.2
C 1s	285.0	61.2
Cl 2p	200.1	0.6
Si 2p	103.7	7.6
2% Co/SiO$_2$–KOH/HCl washed		
Co 2p	778.4	0.2
O 1s	532.9	12.4
N 1s	401.3	4.4
N 1s	398.8	1.7
C 1s	284.9	77.6
Si 2p	103.5	3.7
2% Co/SiO$_2$–HF washed		
Co 2p	778.5	0.4
O 1s	532.3	4.9
N 1s	401.0	4.2
N 1s	398.6	1.7
C 1s	284.7	86.4
F 1s	685.8	0.7
Si 2p	101.9	0.5
2% Fe/SiO$_2$–KOH/HCl washed		
Fe 2p	–	–
O 1s	532.5	6.9
N 1s	401.2	3.9
N 1s	398.7	1.7
C 1s	284.8	87.6
Cl 2p	200.4	0.1
Si 2p	103.3	1.5
2% Ni/SiO$_2$–KOH/HCl washed		
Ni 2p	854.3	0.8
O 1s	532.2	5.5
N 1s	401.2	5.9
N 1s	398.7	1.8
C 1s	284.8	85.4
Si 2p	102.0	0.5
10% Co/SiO$_2$–KOH/HCl washed		
Co 2p	778.4	0.6
O 1s	532.7	14.8
N 1s	401.1	4.5
N 1s	398.8	2.0
C 1s	284.7	74.9
Si 2p	103.3	3.1

energy shoulder, since quarternary nitrogen is simply graphitic nitrogen. This possibility is discussed in more detail elsewhere [23]. The area of this higher binding energy shoulder was therefore lumped with the area of the quarternary nitrogen. All of the samples also had oxygen on the surface which generally fit to one peak, although it is possible that the resolution of the analysis was not high enough to determine if more than one oxygen species is present, which is a distinct possibility.

Table 1 shows the results of XPS analysis for all the washed samples prepared from acetonitrile pyrolysis over silica-based supports. Several important trends are apparent in these results. First, silicon is always present in the samples to some degree (usually as silica evident from the Si 2p peak near 103.5 eV), showing that the KOH wash is not entirely effective at removing silica. Some samples may contain what is believed to be nitrided silicon (BE of 102.0 eV) rather than silica [27]. When HF acid is used as the leaching agent, more silica is removed from the surface. It is possible that some of the silica remaining in the samples is below several layers of carbon, since XPS signal is not entirely limited to the surface. As expected, the samples that contain more silica on the surface also contain more oxygen. A very small amount of chlorine (or fluorine) typically remained in the samples after the wash.

For all the samples, the majority of the surfaces are comprised of carbon. The binding energies are slightly higher than what is typical for elemental carbon due to the doping of the carbon with nitrogen. All of the samples contained a measurable amount of nitrogen. Clearly, the nitrogen content is higher on the surface than what was reported for the bulk of these same samples by TPO elemental analysis, reported elsewhere [26]. From TPO, the nitrogen content was at most 3%, with values closer to 1% being typical for fibers grown from Fe particles (see Ref. [26]). The nitrogen surface enrichment of catalytically grown nitrogen-doped carbon nanofibers has been reported elsewhere [28], and is likely the cause of this discrepancy.

For alumina- and carbon-supported samples reported previously, there was a relation between nanostructure and the ratio of different nitrogen species [21–23]. The cause of this trend was believed to be due to the fact that pyridinic nitrogen is located on the edge plane of carbon, so structures with more edges will inherently have more pyridinic nitrogen. This sort of trend, although not as pronounced, is still apparent in the silica-derived materials. The CN_x deposited on pure silica contains the lowest ratio of pyridinic nitrogen, while the Fe and Co samples contain the highest ratio of pyridinic nitrogen. Surprisingly the Ni sample contains the most nitrogen, but the lowest ratio of pyridinic nitrogen.

The XPS analysis results for the HCl washed magnesia-derived CN_x samples are shown in Table 2. Only a small amount of magnesia remained in the treated and washed pure magnesia-

Table 2
XPS analysis results for CN_x formed from acetonitrile pyrolysis over magnesia supports and washed with HCl acid

Region	BE (eV)	Composition (%)
MgO–HCl washed		
O 1s	532.0	3.4
N 1s	401.1	6.5
N 1s	398.5	2.5
C 1s	284.8	86.1
Mg 2p	50.2	0.1
2% Co/MgO–HCl washed		
Co 2p	780.3	0.5
O 1s	531.9	2.9
N 1s	401.1	5.5
N 1s	398.8	2.2
C 1s	284.7	89.0
Mg 2p	–	–
2% Fe/MgO–HCl washed		
Fe 2p	–	–
O 1s	531.8	3.7
N 1s	401.1	5.1
N 1s	398.4	2.3
C 1s	284.7	89.0
Mg 2p	–	–
2% Ni/MgO–HCl washed		
Ni 2p	854.5	0.3
O 1s	532.4	3.6
N 1s	401.1	3.1
N 1s	398.7	1.3
C 1s	284.6	91.7
Mg 2p	–	–

derived sample. The metal-doped samples were completely free of magnesia after being washed. Chlorine was not detected in the samples. Again most of the surface was made up of carbon in each case, with a slightly higher binding energy than pure elemental carbon. Around 3% oxygen was present in all of the samples.

The nitrogen contents and the relative ratios of nitrogen species varied from sample to sample. The largest nitrogen content was found in CN_x that had been deposited on pure MgO. However, this sample contained a low ratio of pyridinic-to-quarternary nitrogen. Based on the nanostructure of this sample reported previously, the low ratio of pyridinic nitrogen could be expected since the sample did not have significant edge plane exposure. The only structures present were cube-shaped shells of carbon. The sample was not highly graphitic, and had many defects, which could explain the presence of some pyridinic nitrogen. The Fe and Co samples both had structures that would be expected to have exposed edges, and these samples had a higher pyridinic nitrogen ratio. The Ni sample also had a similar ratio of pyridinic-to-quarternary nitrogen, although one would not predict this from its nanostructure. The total nitrogen content of the Ni sample is much lower than the other samples. Still, all of the samples have a higher nitrogen content on the surface than in the bulk when one compares XPS analyses to elemental composition determined by TPO.

Although the carbon- and alumina-derived samples showed a strong correlation between pyridinic nitrogen and nanostructure, this is not necessarily the case for the silica- and magnesia-derived CN_x just discussed. Further, despite the fact that Fe-doped samples have a similar nanostructure regardless of the support used, the CN_x formed from alumina supported Fe has a much higher content of pyridinic nitrogen than the other Fe samples. Several hypotheses could explain these trends. First, XPS signal is not entirely limited to surface, since subsurface layers will contribute to the analysis to some extent (on the order of 5 nm). Fibers with thin walls have a higher percentage of atoms on the surface than thicker fibers. Thus, the analysis of samples containing thicker fibers may be diluted more by subsurface layers than samples containing fibers with walls that are so thin that there are not enough subsurface layers to dilute the analysis. This would explain why the CN_x from Fe/Al_2O_3 (with smaller fibers) has a higher pyridinic nitrogen ratio than CN_x of the same nanostructure formed from Fe supported on silica or magnesia.

Second, it is possible for pyridinic nitrogen to be present at defects in the carbon plane in addition to being located at the edge of a plane. Therefore, some of the precursors could catalyze the formation of pyridinic nitrogen by means other than orientation of carbon planes within the fiber. Since all of the fibers contain pyridinic nitrogen to some extent, despite the fact that some have structures with little or no edge exposure such as the cubes formed on MgO, this hypothesis may be true to some extent. Samples that have a structure with more edge exposure could still account for more pyridinic nitrogen in this case. It should be mentioned that Trasobares et al. [28] noted that more pyridinic nitrogen formed from Fe particles than Ni particles, but the researchers did not attribute this observation to any nanostructure difference.
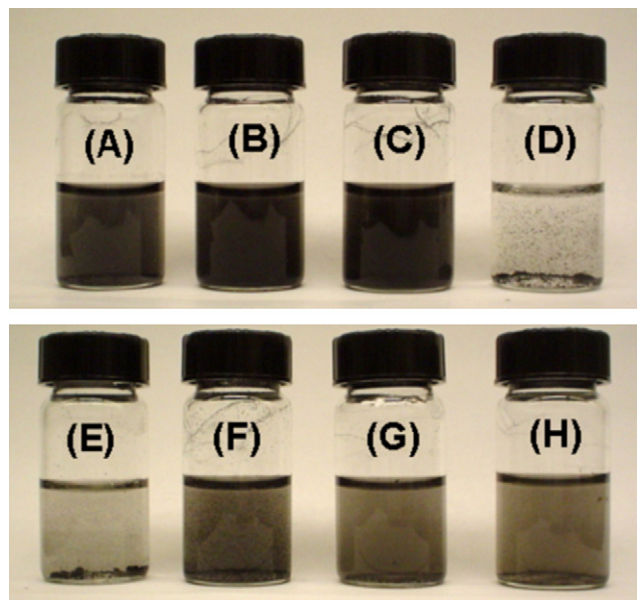
Fig. 3. Hydrophobicity testing for CN_x prepared from CH_3CN pyrolysis over (A) pure MgO, (B) 2% Fe/MgO, (C) 2% Co/MgO, (D) 2% Ni/MgO, (E) pure SiO_2, (F) 2% Fe/SiO_2, (G) 2% Co/SiO_2, and (H) 2% Ni/SiO_2.

A third possibility is that other forms of CN_x, such as amorphous carbon, that cannot be quantified easily by TEM or other means is contributing to the XPS analysis. Amorphous particles were seen in all the samples (although not as abundant as the fibers). Additionally, in the metal-doped MgO samples, the nano-cube structures were observed along with the fibers and likely contributed to the XPS analysis to some extent.

3.2. Hydrophobicity testing

The dispersibility of CN_x samples in water was compared as a measure of hydrophobicity, similar to what was conducted on the alumina-derived samples reported previously [22]. For these tests, 1 mg of sample was sonicated in 10 mL of water for 30 min, then a photograph was taken within 1 min. The photographs for the silica- and magnesia-derived CN_x are shown in Fig. 3. The magnesia samples were similar to the results obtained from the alumina samples. The stacked cup structured carbon formed from Fe and Co particles was the easiest to disperse, while the broken MWNTs formed from Ni particles did not disperse as

well. MWNTs are known to be hydrophobic and are therefore difficult to disperse in water. For the CN_x grown from silica, none of the samples dispersed particularly well in water. These samples all contained some silica on the surface determined from XPS, and a large amount of silica in the bulk, as was determined from TPO/TGA experiments, so this may be a contributing factor to this observation.

3.3. Electrochemical testing

To determine how the samples would perform in a PEM fuel cell, the conductivity was measured using an in-house built set-up described previously, and the ORR activity and selectivity were measured with a RRDE set-up. The results for all of the washed samples are shown in Table 3. Initially, a potential drop method was used to compare activities, where the potential at which the ORR current peaks while the sample is under 0 rpm of rotation is reported as a measure of activity. More active samples peak at higher values. As a reference, a commercial 20 wt% Pt/VC catalyst peaked at 750 mV versus NHE. Later in this section other activity comparison techniques will be discussed, after we point out some obvious trends in activity.

Unlike pure alumina, the CN_x deposited on pure silica and magnesia supports did not form nanofibers, and likewise, were not highly active for the ORR. The pure silica sample had very poor conductivity as well. This sample still contained a large amount of silica after being washed, as TPO/TGA experiments indicated [26].

The Ni-doped supports did not lead to highly active CN_x either. The fibers formed from Ni (regardless of the support used) were mostly of a nanostructure with a low number of edge planes exposed, such as broken MWNTs. In the case of CN_x from Ni/SiO_2 the activity and conductivity were significantly higher than the CN_x deposited on pure silica. There was little difference between the properties of CN_x prepared on pure MgO compared to Ni/MgO.

The CN_x samples with the highest activity were consistently formed from supported Fe and Co particles. These samples also had good conductivity. The conductivity of Vulcan XC-72 was measured to be 71 S/m in the same set-up under the same conditions. The CN_x–Co/SiO_2 samples and the CN_x–Fe/MgO sample all had high activity and conductivity within a factor of three of Vulcan carbon. The most active sample was formed from

Table 3
Electrochemical testing results for CN_x formed from silica and magnesia supports

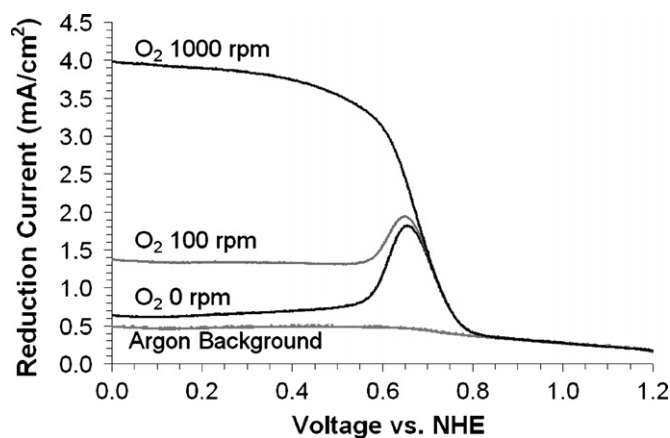| Support	Metal	BET SA (m^2/g)	Conductivity (S/m)	ORR peak (mV vs. NHE)	Average, n
SiO$_2$	–	290	0.2	100	3.3
SiO$_2$	2% Fe	255	11	655	3.95
SiO$_2$	2% Co	465	26	615	3.7
SiO$_2$	2% Co (HF washed)	–	–	570	3.92
SiO$_2$	10% Co	214	26	640	3.6
SiO$_2$	2% Ni		7	405	3.7
MgO	–	180	8	370	3.3
MgO	2% Fe	220	32	580	3.8
MgO	2% Co	280	3	570	3.7
MgO	2% Ni	130	12	400	3.3

Fig. 4. Example of reduction currents for CN_x–Fe/SiO$_2$.

acetonitrile pyrolysis over 2% Fe/SiO$_2$. The sample contained larger diameter fibers (average of 62 nm), mostly of a compartmentalized stacked cup structure (71% of the fibers) as reported previously [26]. The activity of this sample was within a 100 mV potential drop of a state-of-the-art 20 wt% Pt/VC commercial catalyst tested in the same set-up using the same conditions. The CN_x prepared from Fe/SiO$_2$ was also almost completely selective for complete oxygen reduction to water, as will be discussed.

To verify how we obtained the activity testing results, Fig. 4 shows an example of raw data collected for the CN_x–Fe/SiO$_2$ sample. In argon sparged electrolyte only the double-layer capacitance creates a current. In the presence of oxygen, additional current due to the ORR is apparent. Under 0 rpm of rotation in O$_2$, the peak in current at 650 mV is apparent while the onset of current is seen at 830 mV. To obtain selectivity data, currents for the ring and disk while the sample was under 100 rpm of rotation were compared. The magnitudes of the reduction currents for the ring and the disk for the CN_x–Fe/SiO$_2$ sample are shown in Fig. 5. The parameter n was calculated in the mass transfer limited region (where the currents leveled out), using
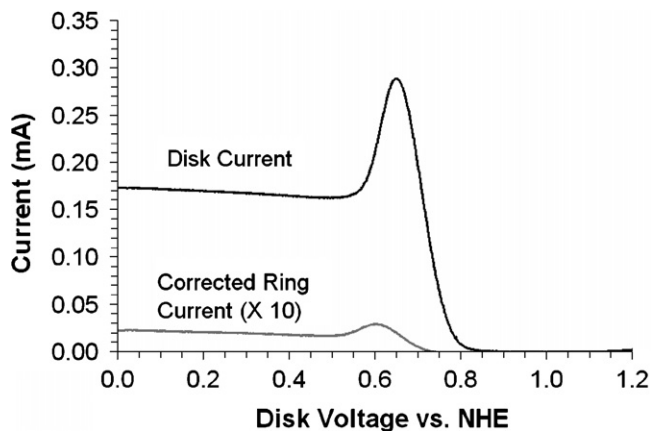
the following equation:

$$n = \frac{4I_D}{I_D + (I_R/N)}$$

where I_D is the disk current, I_R the ring current, and N is the ring collection efficiency reported by the manufacturer to be 0.20.

As seen in Table 3, very little peroxide was formed on the CN_x–Fe/SiO$_2$ sample, demonstrating the ability of these alternative catalysts to completely reduce oxygen to water. In general, there is an apparent loose correlation between activity for the ORR and selectivity of the materials for the complete four-electron reduction to water. The highest values for n are generally samples with high activity. One particular outlier from this trend in the sample prepared using 10 wt% Co/SiO$_2$. While this sample had high activity, its selectivity was rather low, at only $n = 3.6$. This could be related to the large amount of cobalt in this sample. Researchers generally report that catalysts prepared from the pyrolysis of cobalt-containing precursors have poorer selectivity for the four-electron ORR compared to samples prepared from the pyrolysis of Fe precursors [5]. This includes precursors, such as organic macrocycles, polymers, or nitrogen-containing hydrocarbon feeds. Therefore, it is possible that Co is part of an active site for hydrogen peroxide formation, and adding more cobalt increases selectivity to peroxide. The activity for the complete ORR would then be attributed to the nanostructured CN_x formed from the Fe or Co particles.

Washing the Co/SiO$_2$ derived CN_x with HF acid did not affect activity, however, it did improve selectivity for the four-electron reduction. The only significant change in surface properties that were brought about by the HF acid wash was the removal of additional silica, as determined by XPS. Interestingly, the HF wash had a stark effect on the TPO profile of the sample (see Fig. 6). Although the onset of oxidation took place at about the same temperature for both samples, the low temperature feature was much more prominent over the sample washed with HF, which may be due to surface oxidation. Most of the nitrogen oxidation also took place at low temperature region. The bulk of carbon oxidation, on the other hand, took place in the 500–700 °C region. Over the sample which was washed first with KOH and then with HCl, the low temperature oxidation seemed to be suppressed. It is conceivable that K or Cl anions that may be left on the surface from the wash may have an inhibitive effect. Such effects of K and Cl anions on various oxidation reactions have been reported earlier [29–33]. While using HF acid had very little effect on the properties measured by XPS and TPO elemental analysis, from the differences in the TPO profile and the selectivity, it is apparent that using an alternative wash can play a role in the final properties of the catalyst. Based on these results, in future studies it may be important to consider the effect of the wash on the surface properties of the carbon. Certainly, oxidation of the carbon surface could be one anticipated effect of a strong acid wash. Additionally, any effect of modifiers, such as Cl or F, should be considered.

Another useful method for comparing activities, which can also be used to obtain more fundamental data, is Tafel plot evaluation. To compare the performance of the most active sample to the most active alumina-derived sample, and to a commercial
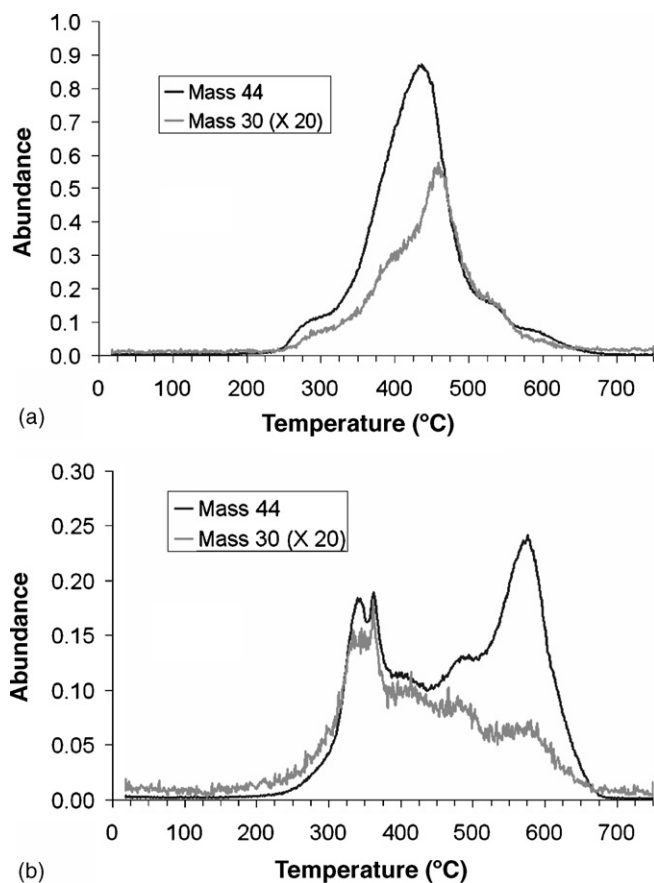

Fig. 5. RRDE reduction currents for CN_x–Fe/SiO$_2$. The argon baseline was subtracted, the electrodes were rotating at 100 rpm in O$_2$ saturated electrolyte, and the ring potential was held at 1.2 V.

Fig. 6. TPO products detected by the mass spectrometer for CN_x prepared from acetonitrile pyrolysis over 2% Co/SiO$_2$: (a) KOH and HCl washed, and (b) HF washed.

Table 4
Tafel plot results for CN_x formed from silica and magnesia supports

Sample	Tafel slope (mV/dec)	Voltage at 0.1 mA/cm^2 (mV vs. NHE)
Commercial 20 wt% Pt/VC	−70	880
CN_x–Al$_2$O$_3$	−146	630
CN_x–SiO$_2$	−213	320
CN_x–MgO	−204	550
CN_x–Co/SiO$_2$	−74	700
CN_x–Co/SiO$_2$ (HF washed)	−72	660
CN_x–Co (10 wt%)/SiO$_2$	−81	720
CN_x–Co/MgO	−71	675
CN_x–Fe/Al$_2$O$_3$	−60	785
CN_x–Fe/SiO$_2$	−59	780
CN_x–Fe/MgO	−63	720
CN_x–Ni/Al$_2$O$_3$	−124	450
CN_x–Ni/MgO	−125	520

The Tafel slopes for all the samples tested are shown in Table 4. The slopes varied significantly for the array of samples, and showed a remarkably strong correlation to the metal used in catalyst preparation. All of the Fe-derived samples had a Tafel slope near −60 mV/dec, the Co samples had a slope between −71 and −81 mV/dec, and the less active samples had much higher slopes. The slope for the commercial platinum catalyst was measured to be −70 mV/dec, and similar values for platinum catalysts are often reported in the literature [16,34]. The less active catalysts had much higher slopes. The slope of a Tafel plot is dependant on the nature of the rate limiting charge transfer in the reduction mechanism [35]. Thus these different slopes indicate large differences in the dependence of the rate limiting charge transfer on voltage, likely resulting from differences in the mechanism. The intermediate slope values could results from competing mechanisms within a sample.

It is not clear whether or not edge plane exposure differences could account for the different slopes. Several modeling studies have examined oxygen reduction on nitrogen-doped carbon edge planes [36,37], and the basal plane [38]. Only reduction to peroxide occurred on the basal plane [38]. Thus, one possibility that could explain the activity, selectivity, and Tafel slope observations is differences in edge plane exposure. A second distinct possibility proposed by other researchers is that the metal becomes an additional active site (beyond the active nitrogen-doped carbon), and this metal-based site improves activity and selectivity [39–41].

Also reported in Table 4 is the voltage at which 0.1 mA/cm^2 of reduction current was achieved. Some researchers report the ORR current "take-off" voltage, however, we believe that reporting a "take off" voltage is somewhat subjective. The voltage value at 0.1 mA/cm^2 essentially provides a less subjective measure of the voltage at which the reduction current starts to become undoubtedly significant and measurable. Thus, comparing these values to one another can be thought of as a potential drop comparison. The trends in these values are therefore similar to the trends observed when comparing the ORR peak voltage discussed earlier.

20% Pt catalyst (Electrochem, EC-20-PTC), Tafel plots were constructed, and are shown in Fig. 7. Data for these plots were taken from the kinetic controlled ORR current of the samples while under 1000 rpm of rotation in O$_2$. The slopes of the non-metal catalysts are similar to the commercial catalyst. On an equal current basis, there is only an additional 100 mV potential drop.
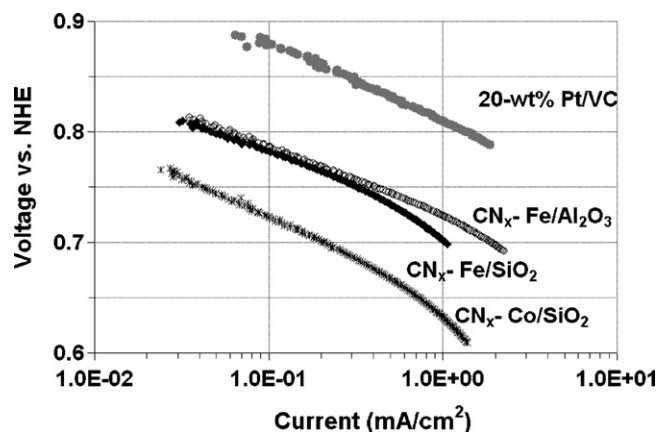

Fig. 7. Tafel plots of most active CN_x catalysts prepared from supported Fe compared to commercial 20 wt% Pt/VC.

4. Conclusions

Nitrogen-containing carbon nanostructures were prepared from the decomposition of acetonitrile at 900 °C over silica and magnesia supports. For the carbon grown from supported Fe and Co particles, compartmentalized fibers with a stacked cup structure predominantly formed, while mostly broken multi-walled nanotubes formed from Ni particles. These observations are consistent with the structures formed from alumina supported Fe and Ni. The samples were all enriched with nitrogen on the surface, and the Fe- or Co-derived fibers generally had higher pyridinic nitrogen contents. Additionally, the stacked cup structured fibers were generally less hydrophobic than MWNTs. Both these surface properties are likely related to edge plane exposure of the carbon.

The nanostructure and surface properties of these new samples were related to electrocatalytic activity. Activity for the ORR was highest over CN_x fibers grown from supported Fe and Co particles, both of which had the compartmentalized stacked cup structures that would be expected to have a higher degree of edge plane exposure than MWNTs. The most active materials were generally the most selective catalysts as well. Moreover, from Tafel plot slopes a trend was observed depending on the precursor metal used to prepare the CN_x. The magnitude of the Tafel slope was smallest for the samples prepared from Fe or Co precursors, and was similar to a commercial platinum-based catalyst. The most active alternative non-noble metal catalysts were comparable in activity (less than 100 mV potential drop) and selectivity to state-of-the-art platinum catalysts. The conductivity of these materials were slightly less than, but still comparable to materials used in PEM fuel cell electrodes. Thus, these non-precious metal cathode catalysts show good potential for replacing platinum in automotive applications.

Acknowledgements

References

[1] S. Srinivasan, in: O.J. Murphy, S. Srinivasan, B.E. Conway (Eds.), Electrochemistry in Transition: From the 20th to the 21st Century, Plenum, NY, 1992, pp. 577–602.

[2] H.A. Gasteiger, S.S. Kocha, B. Sompalli, F.T. Wagner, Appl. Catal. B: Environ. 56 (2005) 9–35.

[3] M. Bron, J. Radnik, M. Fieber-Erdmann, P. Bogdanoff, S. Fiechter, J. Electroanal. Chem. 535 (2002) 113–119.

[4] M. Bron, S. Fiechter, P. Bogdanoff, H. Tributsch, Fuel Cells Fundam. Syst. 2 (2002) 137.

[5] P.H. Matter, E.J. Biddinger, U.S. Ozkan, in: J.J. Spivey (Ed.), Catalysis, vol. 20, The Royal Society of Chemistry, Cambridge, UK, submitted for publication.

[6] R. Jansinski, Nature 201 (1964) 1212.

[7] R. Jansinski, J. Electrochem. Soc. 112 (1965) 526–528.

[8] H. Jahnke, M. Schonborn, G. Zimmerman, Fortschr. Chem. Forsch. 61 (1976) 133.

[9] J.H. Zagal, in: W. Vielstich, H. Gasteiger, A. Lamm (Eds.), Handbook of Fuel Cells—Fundamentals, Technology and Applications, vol. 2, John Wiley and Sons Ltd., 2003, Electrocatalysis.

[10] F. Jaouen, S. Marcotte, J.-P. Dodelet, G. Lindbergh, J. Phys. Chem. B 107 (2003) 1376–1386.

[11] R. Cote, G. Lalande, D. Guay, J.P. Dodelet, G. Denes, J. Electrochem. Soc. 145 (1998) 2411.

[12] M. Lefevre, J.P. Dodelet, P. Bertrand, J. Phys. Chem. B 104 (2000) 11238.

[13] G. Faubert, R. Cote, D. Guay, J.P. Dodelet, G. Denes, C. Poleunis, P. Bertrand, Electrochim. Acta 43 (1998) 1969.

[14] J. Fournier, G. Lalande, R. Cote, D. Guay, J.P. Dodlet, J. Electrochem. Soc. 144 (1997) 218.

[15] S. Gupta, D. Tryk, I. Bae, W. Aldred, E. Yeager, J. Appl. Electrochem. 19 (1989) 19.

[16] S. Gojkovic, S. Gupta, R. Savinell, J. Electroanal. Chem. 462 (1999) 63–72.

[17] J.A.R. van Veen, J.F. van Baar, K.J. Kroese, Chem. Soc., Faraday Trans. I 77 (1981) 2827.

[18] G. Lalande, R. Cote, D. Guay, J.P. Dodelet, L.T. Weng, P. Bertrand, Electrochim. Acta 42 (1997) 1379.

[19] E. Yeager, Electrochim. Acta 29 (1984) 1527–1537.

[20] M. Lefevre, J.-P. Dodelet, Electrochim. Acta 48 (2003) 2749–2760.

[21] P.H. Matter, U.S. Ozkan, Catal. Lett. 109 (2006) 115–123.

[22] P.H. Matter, E. Wang, M. Arias, E.J. Biddinger, U.S. Ozkan, J. Phys. Chem. B, in press.

[23] P.H. Matter, L. Zhang, U.S. Ozkan, J. Catal. 239 (2006) 83–96.

[24] S. Maldonado, K.J. Stevenson, J. Phys. Chem. B 109 (2005) 4707–4716.

[25] S. Maldonado, K.J. Stevenson, J. Phys. Chem. B 108 (2004) 11375–11383.

[26] P.H. Matter, E. Wang, U.S. Ozkan, J. Catal., in press.

[27] J.F. Moulder, W.F. Strickle, P.E. Sobol, K.D. Bomben, Handbook of Photoelectron Spectroscopy, Perkin-Elmer Corporation, Eden Prairie, MN, 1992.

[28] S. Trasobares, O. Stephan, C. Colliex, W.K. Hsu, H.W. Kroto, D.R.M. Walton, J. Chem. Phys. 116 (2002) 8966–8972.

[29] R.B. Watson, U.S. Ozkan, J. Catal. 191 (2000) 12–29.

[30] R.B. Watson, U.S. Ozkan, J. Phys. Chem. 106 (2002) 6930–6941.

[31] R.B. Watson, U.S. Ozkan, J. Mol. Catal. A: Chem. 194 (2003) 115–135.

[32] R.B. Watson, S. Lashbrook, U.S. Ozkan, J. Mol. Catal. 208 (2004) 233–244.

[33] C. Liu, U.S. Ozkan, J. Mol. Catal. A: Chem. 220 (2004) 53–65.

[34] K. Kinoshita, Electrochemical Oxygen Technology, John Wiley and Sons Inc., 1992.

[35] A.J. Bard, L.R. Faulkner, Electrochemical Methods: Fundamentals and Applications, John Wiley and Sons Ltd., NY, 2001.

[36] V.V. Strelko, N.T. Kartel, I.N. Dukhno, V.S. Kuts, R.B. Clarkson, B.M. Odintsov, Surf. Sci. 548 (2004) 281–290.

[37] V.V. Strelko, V.S. Kuts, P.A. Thrower, Carbon 38 (2000) 1499–1525.

[38] R.A. Sidik, A.B. Anderson, N.P. Subramanian, S.P. Kumaraguru, B.N. Popov, J. Phys. Chem. B 110 (2006) 1787–1793.

[39] M. Lefevre, J.P. Dodelet, P. Bertrand, J. Phys. Chem. B 106 (2002) 8705–8713.

[40] M. Jain, S.-h. Chou, A. Siedle, J. Phys. Chem. B 110 (2006) 4179–4185.

[41] H. Schulenburg, S. Stankov, V. Schuenemann, J. Radnik, I. Dorbandt, S. Fiechter, P. Bogdanoff, H. Tributsch, J. Phys. Chem. B 107 (2003) 9034–9041.